Title
Rebar graphene.

Journal
ACS nano, 8(5)

ISSN
1936-0851

Authors
Yan, Zheng
Peng, Zhiwei
Casillas, Gilberto
et al.

Publication Date
2014-05-01

DOI
10.1021/nn501132n

Peer reviewed

Rebar Graphene

Zheng Yan,[†] Zhiwei Peng,[†] Gilberto Casillas,[∥] Jian Lin,[‡,§] Changsheng Xiang,[†] Haiqing Zhou,[†] Yang Yang,[†,‡] Gedeng Ruan,[†] Abdul-Rahman O. Raji,[†] Errol L. G. Samuel,[†] Robert H. Hauge,[†,‡,⊥] Miguel Jose Yacaman,[∥] and James M. Tour[†,‡,§,*]

[†]Department of Chemistry, [‡]Richard E. Smalley Institute for Nanoscale Science and Technology, [§]Department of Materials Science and NanoEngineering, Rice University, 6100 Main Street, Houston, Texas 77005, United States, [∥]Department Physics and Astronomy, University of Texas at San Antonio, One UTSA Circle, San Antonio, Texas 78249, United States, and [⊥]Chemistry Department, Faculty of Science, King Abdulaziz University, P.O. Box 80203, Jeddah 21589, Saudi Arabia

ABSTRACT As the cylindrical sp^2-bonded carbon allotrope, carbon nanotubes (CNTs) have been widely used to reinforce bulk materials such as polymers, ceramics, and metals. However, both the concept demonstration and the fundamental understanding on how 1D CNTs reinforce atomically thin 2D layered materials, such as graphene, are still absent. Here, we demonstrate the successful synthesis of CNT-toughened graphene by simply annealing functionalized CNTs on Cu foils without needing to introduce extraneous carbon sources. The CNTs act as reinforcing bar (rebar), toughening the graphene through both $\pi-\pi$ stacking domains and covalent bonding where the CNTs partially unzip and form a seamless 2D conjoined hybrid as revealed by aberration-corrected scanning transmission electron microscopy analysis. This is termed rebar graphene. Rebar graphene can be free-standing on water and transferred onto target substrates without needing a polymer-coating due to the rebar effects of the CNTs. The utility of rebar graphene sheets as flexible all-carbon transparent electrodes is demonstrated. The in-plane marriage of 1D nanotubes and 2D layered materials might herald an electrical and mechanical union that extends beyond carbon chemistry.

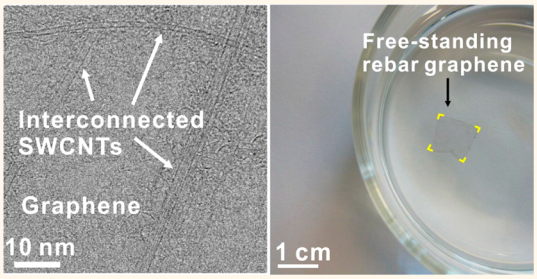

KEYWORDS: reinforced graphene · SWCNTs · free-standing · synergistic effect · chemical vapor deposition

Following the pioneering research by Geim and colleagues,[1] graphene has been intensively studied over the past decade.[2,3] Since many of the rapidly realizable targets have been reached, researchers have now started to address the remaining challenges by combining graphene with other materials.[4−11] For example, graphene and hexagonal boron nitride (h-BN) lateral heterostructures have been successfully synthesized for the design of atomically thin circuitry.[5] Vertically stacked graphene/h-BN hybrids can be directly used for the fabrication of high-mobility graphene transistors.[6,7] Most recently, we have shown the synthesis of 3D graphene/vertical CNT seamless structures for energy storage and field-emission emitters.[8,9] However, the studies of planar CNT/graphene hybrids are limited.

In this paper, we describe the simple synthesis of planar CNT/graphene hybrid sheets. Just as macroscopic reinforcing bar (rebar) can toughen materials, the planar CNT/graphene is a toughened form of 2D material, and it is termed here as "rebar graphene". This research has made the following contributions to the graphene community: (1) The concept of using CNTs to in-plane reinforce graphene was established. In contrast to general chemical vapor deposition (CVD) graphene, CNT-reinforced graphene was transferred onto target substrates without needing a polymer coating. (2) Rebar graphene was fabricated by simply annealing functionalized CNTs on Cu foils without introducing extraneous carbon sources. According to our recent research, solid carbon sources have served as sources for single-layer graphene growth on Cu.[10,11] In this special case, the CNTs functional groups decomposed and formed single-layer graphene on Cu during the annealing process. Moreover, the as-made CNT−graphene hybrid material demonstrated ambipolar electronic behavior. (3) The interfaces between single-walled carbon nanotubes (SWCNTs) and graphene were investigated at atomic resolution using scanning transmission electron microscopy (STEM). Two types of interfaces, covalent bonding and $\pi-\pi$ stacking, were revealed. (4) Due to the synergistic effects, the as-fabricated rebar graphene not only was free-standing on water and allowed for polymer-free transfer onto other substrates, but also showed improved sheet resistance

* Address correspondence to tour@rice.edu.

Received for review February 25, 2014 and accepted April 2, 2014.

Published online April 02, 2014
10.1021/nn501132n

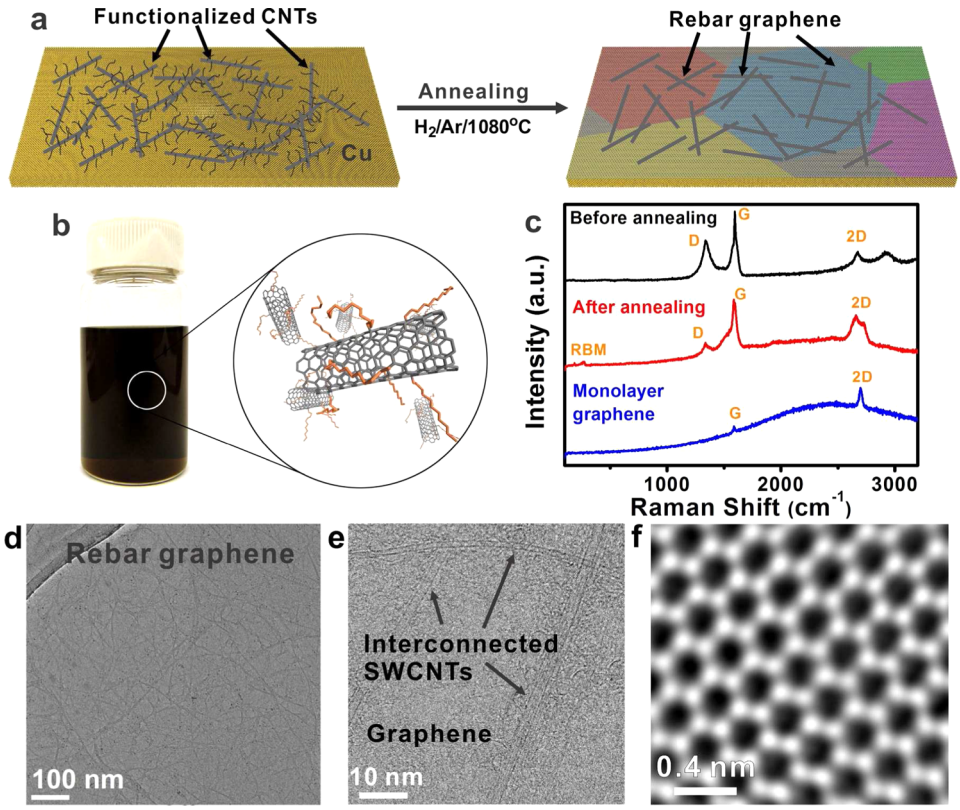

Figure 1. Synthesis and spectroscopic analysis of rebar graphene sheets. (a) The synthesis of rebar graphene sheets was achieved on Cu foils by heating functionalized CNTs in a H_2/Ar atmosphere at 1080 °C for 15 min. In this case, the as-grown graphene was polycrystalline.[14] (b) A typical optical image of the DF-SWCNT chloroform solution and the related structural models. (c) Raman spectra showing that high-quality rebar graphene sheets were successfully synthesized by annealing DF-SWCNT-covered Cu foils. The blue curve is a typical Raman spectrum of monolayer graphene on Cu. The strong backgrounds of the Raman spectra are from the photoluminescence of Cu. The Raman spectra were recorded using 514 nm excitation. (d and e) TEM and BF-STEM images indicating the formation of interconnected SWCNT networks in rebar graphene sheets. (f) An atomic-resolution ADF-STEM image showing the defect-free hexagonal lattice of monolayer graphene, indicating the high-quality monolayer nature of the graphene in the rebar graphene sheets.

at higher transparency as compared to general polycrystalline CVD graphene.

RESULTS AND DISCUSSION

Figure 1a schematically shows the process of using functionalized CNTs as raw materials on Cu foils. Dodecyl-functionalized single wall carbon nanotubes (DF-SWCNTs) were used to demonstrate the synthesis of rebar graphene. The SWCNTs were HiPco-produced and purified.[12] DF-SWCNT chloroform solutions were prepared using the method as reported[13] (Figure 1b). The synthesis of rebar graphene was achieved as follows. The 200 μL DF-SWCNT $CHCl_3$ solutions (3.2 mg/mL) were dispersed on the pretreated Cu foils (1 cm × 1 cm)[14] using a spin-coater at 500 rpm for 10 s. Then, the Cu foils were loaded into a CVD furnace and annealed for 15 min at 1080 °C with the flow rate of H_2 at 50 sccm, the flow rate of Ar at 500 sccm, and the chamber pressure at 7 Torr. No exogenous carbon growth source was added. After an annealing step, the Cu foils were quickly removed from the hot region of the CVD chamber using a magnetic rod and then cooled to room temperature. Detailed rebar graphene growth procedures are described in the Supporting Information.

Raman spectroscopy was first used to investigate the formation of rebar graphene on Cu foils using 514 nm excitation. The Raman spectra in Figure 1c are characteristic of 10 locations recorded on 1 cm^2 of the sample. Pristine SWCNTs exhibit three typical bands: a radial breathing mode (RBM) at ~250 cm^{-1}, a G band at ~1590 cm^{-1}, and a weak D band at 1340 cm^{-1}, with the intensity ratio of D to G bands less than 0.1.[15] The black curve in Figure 1c is a typical Raman spectrum of DF-SWCNTs deposited on Cu before annealing. The intensity ratio of the D band at ~1340 cm^{-1} to the G band at ~1590 cm^{-1} was ~0.5 and no obvious RBMs could be detected at ~250 cm^{-1}, indicating that sp^2 structures of SWCNTs were distorted due to the covalent bonds of the dodecyl groups.[13] The red curve in Figure 1c is a representative Raman spectrum of rebar graphene grown on Cu foils. We can see that RBMs appear at ~250 cm^{-1} after annealing. Moreover, the intensity ratio of the D to G bands decreased to less than 0.1, indicating the presence of few sp^3 carbon atoms or defects.[15] During the

annealing process, SWCNTs could self-heal as the dodecyl groups thermally decomposed and become graphene on Cu, enabling the formation of rebar graphene. The appearance of the RBMs and the decrease of the intensity ratio of D to G bands in the annealed rebar graphene support the suggestion of self-healing of SWCNTs. Moreover, in the 2D band, there is a shoulder at ~2698 cm^{-1}, related to the position of the 2D band of monolayer graphene on Cu (the blue curve in Figure 1c), indicating the dominant monolayer nature of the graphene in the as-made rebar graphene sheets. This was further confirmed by transmission electron microscopy (TEM) characterizations (*vide infra*). Similar results were also recorded by Raman spectroscopy with 633 nm excitation and the representative Raman spectra from 10 locations recorded on 1 cm^2 of the sample are shown in Figure S1. The X-ray photoelectron spectroscopy (XPS) analysis is shown in Figure S2. After annealing, the position of the C 1s peak moves from 284.9 to 284.5 eV, with an asymmetric tailing toward high bonding energy; the full width at half-maximum (fwhm) decreased to ~0.8 from ~1.2 eV, indicating that the sp^3-carbon structures in DF-SWCNTs were transformed into sp^2-carbon-based graphitic structures.[16] No obvious C−N bonding and C−O bonding were observed in Figure S2, confirming the growth of pristine rebar graphene. Representative scanning electron microscope (SEM) images of rebar graphene sheets grown on Cu are shown in Figure S3; no SWCNT bundles were observed in the SEM images, indicating the formation of a 2D hybrid sheet rather than 3D structures.

As-produced rebar graphene was transferred onto c-flat TEM grids (Protochips) for further characterization. Panesl d and e of Figure 1 are typical TEM and bright-field STEM (BF-STEM) images, respectively, of suspended rebar graphene on TEM grids, indicating that individually dispersed SWCNTs formed interconnected networks on continuous graphene sheets to form a new 2D carbon material. More than 10 graphene locations in rebar graphene were investigated using STEM. Typical atomic-resolution STEM images are shown in Figure 1f and Figure S4, indicating low-defect hexagonal lattices of monolayer graphene. These atomic resolution-STEM images, corroborating the above Raman analysis, further confirm the high-quality monolayer nature of the graphene in the rebar graphene. Second-layer graphene islands could be occasionally found and a TEM image of such a location is shown in Figure S5. Due to the different chemical reactivities of graphene and SWCNTs,[17,18] the rebar graphene might have potential applications where the selective modification of graphene or SWCNTs is exploited.

In recent research, the use of polymers such as poly(methyl methacrylate) (PMMA) and polydimethylsiloxane (PDMS) as support layers has become unavoidable for isolating CVD-based graphene,[19−22] graphene-like 2D layered materials[23,24] or in-plane graphene-based heterostructures[5] from the catalyst metal substrates. Surface contaminations from polymer residues have long-been a troublesome issue, limiting the analyses of the intrinsic properties of the carbon materials and retarding their applications in surface chemistry, ultrahigh-speed electronics and biodevices. In this research, we found that the SWCNTs reinforced the rebar graphene, thus enabling polymer-free transfers onto target substrates such as TEM grids and SiO_2/Si wafers (see the Supporting Information for details). Figure 2a is a representative photograph of one rebar graphene sheet, floating on water containing 1% butanol by volume. This free-standing rebar graphene was ~1 cm × 1 cm in size, approximately one-atom-thick, not precoated with any polymer and was ready to be transferred onto other substrates. The grown catalyst substrate, Cu foil, was already etched away using an ammonium persulfate-based etchant solution. Here, butanol was used to lower the surface tension of the water. The butanol residue could be readily removed by vacuum treatment after transferring the rebar graphene sheets onto target substrates. In a control experiment, we found that, without the polymer precoating, both conventional CVD polycrystalline graphene films and millimeter-sized single-crystal graphene[14] broke into small pieces using the same aqueous etchant containing butanol when the substrates were etched away. This underscores that only the rebar graphene hybrid structure can endure on water without destruction. Additionally, TEM images in Figure 2b demonstrate that the nonpolymer transferred rebar graphene sheet had a cleaner surface than that of the PMMA-assisted transferred rebar graphene. Polymer-free transfers could facilitate the uses of rebar graphene in transparent electrode technologies and chemical modification strategies as in sensors and biodevices where trace impurities cause limitations.

We used STEM to explore the reinforcement effects of SWCNTs in rebar graphene transferred onto TEM grids using the polymer-free transfer method (see the Supporting Information for details). Nanometer-sized cracks could occasionally be found in the suspended rebar graphene sheets when butanol was not used to lower the water surface tension. Figure 2c,d shows typical annular dark field STEM (ADF-STEM) images of those cracks. From the ADF-STEM images, it is apparent that several individually dispersed SWCNTs straddle the crack, restraining its further extension. Figure 2e shows an atomic-resolution ADF-STEM image of the region of the suspended SWCNT in Figure 2d indicated by the yellow section, showing a clear moirés pattern with a periodicity at ~0.8 nm. This indicates that the SWCNT is chiral and can be represented by a pair of indices (n, m).[25] By simulating TEM images of SWCNTs with different (n, m) indices (Figure 2f,g and

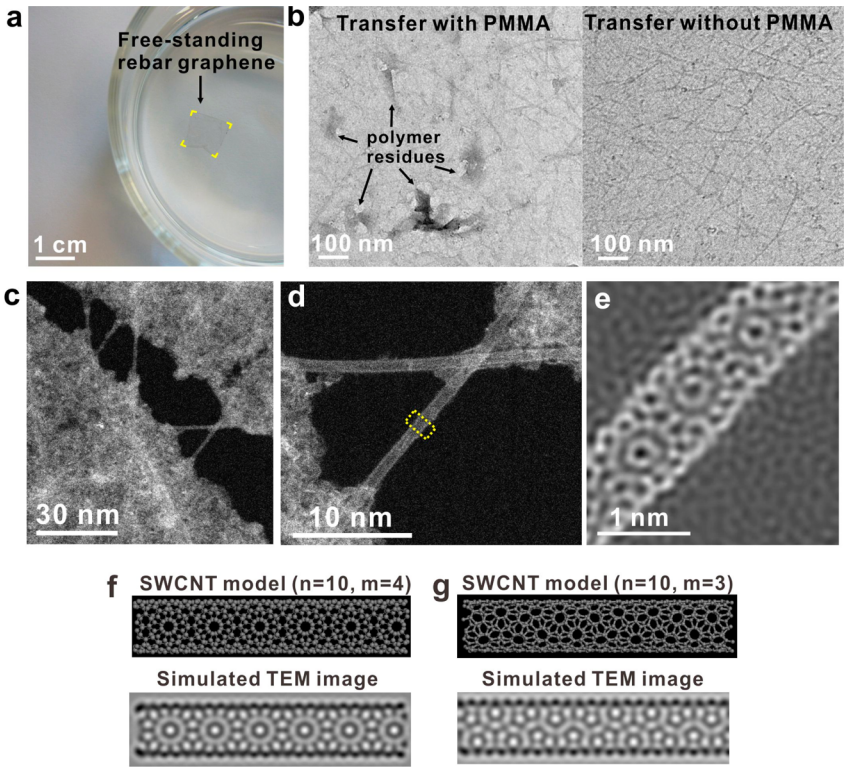

Figure 2. CNT reinforcement in rebar graphene sheets. (a) A free-standing rebar graphene sheet, highlighted in yellow at the corners, floating on water with 1% butanol by volume. The rebar graphene sheet is ~1 cm × 1 cm and not precoated with any polymers. Here, butanol was used to lower the surface tension of water and could be removed by vacuum treatment after transferring the rebar graphene sheets onto the target substrates. (b) TEM images indicating that a conventional PMMA-assisted transferred rebar graphene sheet is dotted with polymer residues (left) and the polymer-free transferred rebar graphene sheet that has a clean surface (right). (c and d) ADF-STEM images of rebar graphene suspended on TEM grids, demonstrating that SWCNTs straddle cracks and work to strengthen the rebar graphene sheet. This sample came from a water float that did not contain 1% butanol to lower the surface tension, thus leading to the formation of small cracks in rebar graphene; it is different than the sample in panel a. The bright contrast in the graphene region originates from hydrocarbon contamination absorbed from the air. (e) An atomic-resolution ADF-STEM image of the region of the SWCNT indicated by the yellow region in panel d, showing a clear moirés pattern with a periodicity at ~0.8 nm. (f and g) Structural models and simulated TEM images of the chiral SWCNT (10, 4) and the chiral SWCNT (10, 3).

Figure S6), we concluded that a SWCNT with indices n = 10 and m = 4 (Figure 2f) best matched the experimental image. The diameter could be calculated (Supporting Information and ref 25), which was ~0.978 nm. However, the measured diameter of this SWCNT by STEM was ~0.864 nm (Figure S7). This diameter shrinkage is evidence that the SWCNT is under tensile stress, demonstrating how SWCNTs reinforce and strengthen rebar graphene sheets and enable their polymer-free transfers.

An interesting question is: how are graphene and SWCNTs connected in the rebar graphene sheets? The graphene–SWCNT interfaces were investigated using STEM; two types of graphene–SWCNT connections, π–π stacking and covalent bonds, were revealed (Figure 3 and Figure S8). Figure 3a is a typical BF-STEM image of π–π stacked graphene–SWCNT interfaces; the structural model is shown in Figure S8a. From Figure 3a, it is apparent that there is no buckling or distortion around the graphene–SWCNT interface, indicating that, in this case, the graphene sheet and the SWCNT are intimately combined together *via* π–π stacking rather than sp^2 or sp^3 bonds. The fast Fourier transform (FFT) patterns of a1 and a2 show the typical hexagonal crystalline structures of monolayer graphene and demonstrate the same rotation angles, meaning the graphene lying on both sides (a1 and a2) of this SWCNT belong to the same monolayer graphene grain.[14] This can be understood if we assume that the SWCNT in this area has a sp^2-carbon bonded graphitic structure without dangling bonds or sp^3-carbon related defects, thus the graphene grew beneath it to form the π–π stacked interface with the SWCNT during the annealing process. Additionally, Figure S8b,c indicates a 6000 count increment in the intensity profile from the graphene region to the SWCNT region, equivalent to the ADF intensity of two graphene layers (Figure S9), which further demonstrates that the graphene and the SWCNT are overlapped via π–π stacking rather than covalent welding. Both images were acquired under the same conditions to ensure the number of counts is the same for both.

Figure 3b,c is typical BF-STEM images of covalent bonding in the rebar graphene. From Figure 3b, as

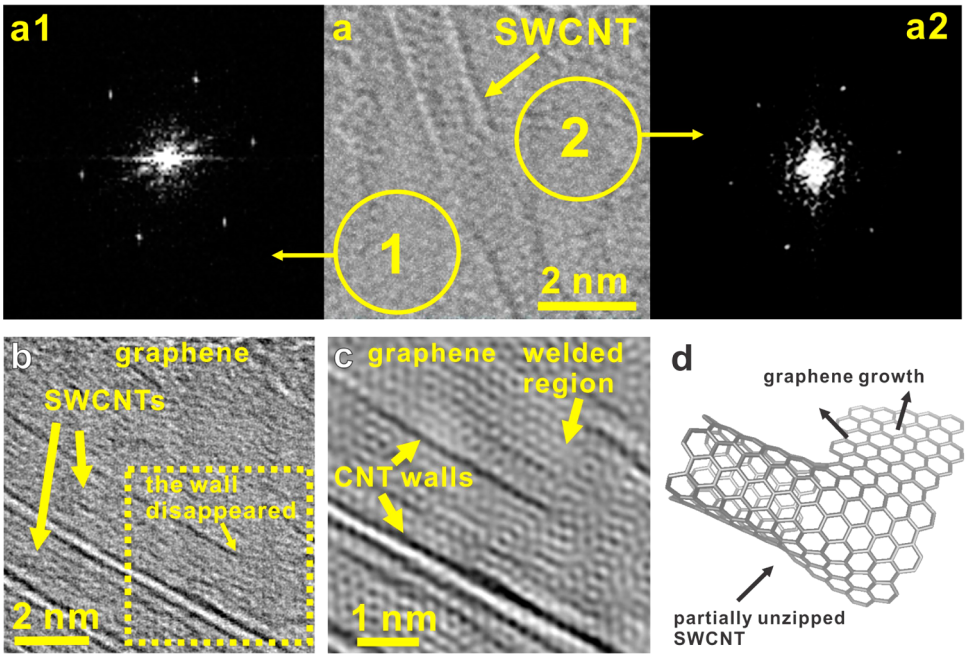

Figure 3. Graphene–SWCNT interfaces in rebar graphene. (a) FFT patterns (a1 and a2) and the BF-STEM image of one $\pi-\pi$ stacked graphene–SWCNT interface. The ADF-STEM-derived intensity profile of similar structures (Figures S8 and S9) further demonstrates the graphene–SWCNT overlapping structures. (b) The BF-STEM image of a covalently bonded graphene–SWCNT interface. (c) The high-resolution image after applying a filter of the FFT in the raw BF-STEM image of the yellow selected area in panel b. The "welded region" refers to the seamless covalent bonding between the SWCNT and the graphene. (d) The scheme for graphene growth from the edges of a partially unzipped SWCNT. This would likely reside on the bottom face of the SWCNT that is in contact with the Cu.

indicated by the area in the yellow square, one SWCNT wall disappeared where the graphene and SWCNT were bonded together in-plane. Figure 3c is a high-resolution BF-STEM image of the region indicated by the yellow square in Figure 3b, showing that graphene and SWCNT are covalently bonded through aromatic rings. The proposed formation mechanism of the covalent bonded interface is as follows: (1) SWCNTs could be partially unzipped due to the etching by the Cu foil at high temperature (Figure 3b,c); (2) the exposed SWCNT edges could capture active carbons for graphene growth[26] (Figure 3d); (3) graphene and SWCNTs are covalently welded together by aromatic rings in the partially unzipped SWCNT regions (Figure 3b,c). In addition, on the basis of the Raman spectrum in Figure 1c, RBMs were detected in the rebar graphene sheets; the intensity ratio of the D to G bands dropped to <0.1, demonstrating the weak etching effects of Cu on SWCNTs because of the low solubility of carbon in Cu (<0.001 atom % at 1000 °C).[27] Thus, $\pi-\pi$ stacked graphene–SWCNT interfaces dominated in rebar graphene sheets synthesized on Cu foils, but there are sufficient amounts of covalently fused regions to render a noticeable toughening.

The electrical transport properties of rebar graphene sheets were evaluated by fabricating Hall bar field effect transistors on SiO_2 (100 nm)/Si substrates (see the Supporting Information for details). The measurements were performed at room temperature at a pressure of less than 10^{-5} Torr. The inset of Figure 4a provides a typical optical image of the as-made Hall bar device based on rebar graphene; its related electrical behaviors are shown in Figure 4a,b. From Figure 4a, a gating effect was observed on this Hall bar device, with the on/off ratio of ~11. Moreover, Figure 4a indicates that the as-made device shows typical ambipolar behavior, meaning that graphene dominated the electronic properties in rebar graphene sheets. The calculated carrier (hole) mobility for the device in the inset of Figure 4a was ~2200 $cm^2 V^{-1} s^{-1}$ at a carrier density of 5×10^{12} cm^{-2} based on the Drude model[28] (Figure 4b). More than five rebar graphene based Hall bar devices were fabricated on SiO_2/Si substrates. All of them had typical ambipolar behavior, with the carrier (hole) mobilities ranging from ~1500 to ~2200 $cm^2 V^{-1} s^{-1}$ at a carrier density of 5×10^{12} cm^{-2}. The mobilities are comparable to those of CVD polycrystalline graphene,[19−21] indicating the high quality of the rebar graphene.

Cu and Ni are the most widely used catalyst metals for the growth of graphene[19−21] and graphene-based heterostructures.[5,23] The influence of these two catalyst substrates on the rebar graphene growth was investigated. From Figure 4c, it is apparent that extending the annealing time has little effect on the synthesis of rebar graphene on Cu foils. Even after annealing DF-SWCNTs on Cu for 3 h at 1080 °C, RBMs were still clearly detected from the as-made hybrid

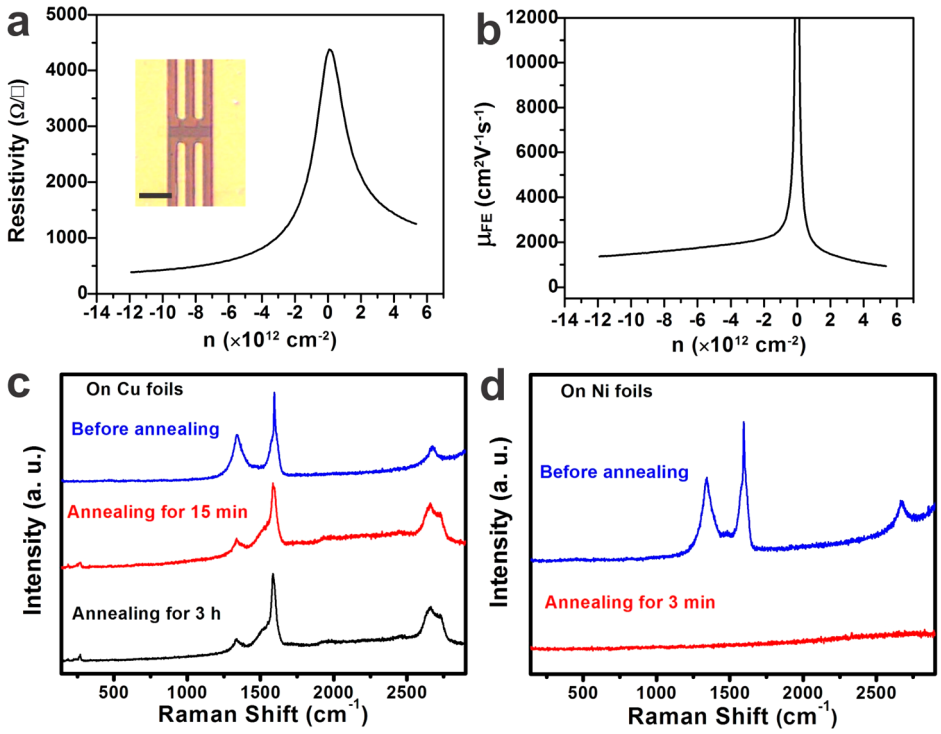

Figure 4. Electrical properties and control growth experiments of rebar graphene on Cu- and Ni-foils. (a) Resistivity as a function of carrier density measured at room temperature. The inset is an optical image of the fabricated rebar graphene Hall bar field effect transistor on a SiO_2/Si substrate; the scale bar is 20 μm. (b) Plot of density-dependent field effect mobility of rebar graphene *vs* carrier density from the device indicated in the inset of panel a. (c) Raman spectra indicating the weak etching ability of Cu on SWCNTs at 1080 °C for 15 min and 3 h. (d) Raman spectra demonstrating the high etching ability of Ni on SWCNTs. Here, DF-SWCNTs were used as raw materials and deposited on surfaces of Cu- and Ni-foils using a spin-coater (see the Supporting Information for details).

material. In contrast, Figure 4d indicates that after annealing DF-SWCNTs on Ni foils for 3 min at 1080 °C and then cooling the sample to room temperature, no carbon-related structures could be detected by Raman spectroscopy. This is because: (1) Ni has a high etching ability on SWCNTs because of its high carbon solubility (~1.3 atom % at 1000 °C).[27] During the annealing process, the DF-SWCNTs were completely dissolved by the Ni. Thus, no SWCNTs could be detected by Raman spectroscopy after annealing. (2) The carbon supplied by DF-SWCNTs was not enough for the precipitation growth of graphene on the Ni foil during the cooling process. Thus, graphene signals were absent after annealing. Considering the low etching ability of Cu and the high etching ability of Ni on SWCNTs, the graphene–CNT interface composition might be controlled in the future using properly designed Ni–Cu alloys as the growth substrates. Furthermore, the grain sizes of rebar graphene are ~10 μm, which are estimated by SAED patterns and similar to those of general Cu-based CVD polycrystalline graphene.[14] The grain sizes might be further improved using Ar-only annealed Cu foils as the growth substrates.[29]

One potential application of graphene and CNTs is as a flexible transparent conductive electrodes because of their high optical transmittance, conductivity and flexibility.[19,30−32] However, general CVD graphene is polycrystalline. Graphene grain boundaries are composed of aperiodic heptagon–pentagon pairs, which degrade electronic conductivity of graphene.[33] In rebar graphene, CNTs form a network (Figure 1d,e) and then serve as bridges across graphene boundaries. Thus, rebar graphene demonstrates improved electronic conductivity when compared to general polycrystalline CVD graphene (Figure S10). DF-SWCNTs, arylsulfonated-SWCNTs and Pluronic 127 (a widely used water-soluble triblock polymer) wrapped multiwalled CNTs (M-grade from NanoTechLabs, Inc.) were used as raw materials to make rebar graphene sheets as all-carbon flexible transparent conductive electrodes (see Figure S10 for details). The optimal growth conditions were used to fabricate the electrodes (see the Supporting Information for details). The rebar graphene sheets derived from Pluronic 127 wrapped multiwalled CNTs had ~95.8% transmittance at 550 nm wavelength with a sheet resistance of ~600 Ω/□, indicating better performance than those of stacked CVD bilayer graphene[30] or CNT films at the same transimittance.[31] Improvements could be expected using predominantly metallic or long SWCNTs as raw materials or applying chemical doping.[32] In addition, if additives could be further introduced into the rebar graphene sheet matrix during the annealing process, such as nitrogen and borane doping, the doped hybrid

material could have potential applications in fuel cells and lithium batteries.

Meanwhile, during the revision of this article, we noticed the publication of vein-membrane like CNT/graphene hybrid structures, which exhibited improved mechanical strength, electrical conductivity, and electron transparency properties.[34]

CONCLUSIONS

In conclusion, we have synthesized planar rebar graphene sheets on Cu foils using functionalized CNTs as raw material. The CNTs strengthen rebar graphene sheets through reinforcement, enabling the polymer-free transfer of the rebar graphene onto target substrates. The graphene–CNT interfaces were investigated using STEM, and two types of connections, $\pi-\pi$ stacking and seamless covalent bonding, were shown. Additionally, the potential application of rebar graphene in flexible transparent conductive electrodes was demonstrated. A wide variety of planar hybrid sheets with interesting properties might be achieved in the future using various carbon, boron nitride and metal chalcogenide nanotubes, and graphene or graphene-like 2D materials.

METHODS

The Raman spectra were recorded with a Renishaw Raman RE01 scope. SEM images were taken using a FEI Quanta 400-field emission gun SEM. TEM characterizations were performed using a 200 kV JEOL FE2100 TEM. STEM images were collected with a JEOL JEM-ARM200F operated at 80 kV equipped with a Cs probe corrector. After the samples were loaded into the microscopic chamber, they were beam-showered for 20 min to avoid contamination. ADF-STEM images were acquired with inner and outer collection semiangles of 33 and 125 mrad, respectively, while the BF-STEM images were acquired with a collection semiangle of 8 mrad. All images were acquired with a convergence semiangle of 24 mrad and a dwell time of 96 μs. The electrical transport properties were measured in a probe station (Desert Cryogenic TT-probe 6 system) under vacuum (10^{-5} to 10^{-6} Torr) and the data were collected by an Agilent 4155C semiconductor parameter analyzer. XPS was performed on a PHI Quantera SXM scanning X-ray microprobe with 100 μm beam size and 45° takeoff angle.

Conflict of Interest: The authors declare no competing financial interest.

Acknowledgment. The Peter M. and Ruth L. Nicholas Post-Doctoral Fellowship of the Smalley Institute for Nanoscale Science and Technology supported Y. Yang. The ONR MURI program (#00006766, N00014-09-1-1066), AFOSR MURI (FA9550-12-1-0035), AFOSR (FA9550-09-1-0581), the National Center for Research Resources (5 G12RR013646-12) and Health Disparities (G12MD007591) from the National Institutes of Health provided funding. The authors also acknowledge the support of NSF-PREM Grant No. DMR 0934218. The authors thank Yuanyue Liu for simulating the structural model of graphene–CNT interfaces in Figure 3d, and also thank W. E. Billups for providing DF-SWCNT chloroform solutions.

Supporting Information Available: Images, spectra and additional experimental procedures. This material is available free of charge *via* the Internet at http://pubs.acs.org.

REFERENCES AND NOTES

1. Novoselov, K. S.; Geim, A. K.; Morozov, S. V.; Jiang, D.; Zhang, Y.; Dubonos, S. V.; Grigorieva, I. V.; Firsov, A. S. Electric Field Effect in Atomically Thin Carbon Films. *Science* **2004**, *306*, 666–669.
2. Geim, A. K.; Novoselov, K. S. The Rise of Graphene. *Nat. Mater.* **2007**, *6*, 183–191.
3. Novoselov, K. S.; Falko, V. I.; Colombo, L.; Gellert, P. R.; Schwab, M. G.; Kim, K. A Roadmap for Graphene. *Nature* **2012**, *490*, 192–200.
4. Geim, A. K.; Grigorieva, I. V. Van der Waals Heterostructures. *Nature* **2013**, *499*, 419–425.
5. Levendorf, M. P.; Kim, C. J.; Brown, L.; Huang, P. Y.; Havener, R. W.; Muller, D. A.; Park, J. Graphene and Boron Nitride Lateral Heterostructures for Atomically Thin Circuitry. *Nature* **2012**, *488*, 627–632.
6. Dean, C. R.; Young, A. F.; Meric, I.; Lee, C.; Wang, L.; Sorgenfrei, S.; Watanabe, K.; Taniguchi, T.; Kim, P.; Shepard, K. L.; *et al.* Boron Nitride Substrates for High-Quality Graphene Electronics. *Nat. Nanotechnol.* **2010**, *5*, 722–726.
7. Yang, W.; Chen, G.; Shi, Z.; Liu, C.; Zhang, L.; Xie, G.; Cheng, M.; Wang, D.; Yang, R.; Shi, D.; *et al.* Epitaxial Growth of Single-Domain Graphene on Hexagonal Boron Nitride. *Nat. Mater.* **2013**, *12*, 792–797.
8. Zhu, Y.; Li, L.; Zhang, C.; Casillas, G.; Sun, Z.; Yan, Z.; Ruan, G.; Peng, Z.; Raji, A. O.; Kittrell, C.; *et al.* A Seamless 3-Dimensional Carbon Nanotube Graphene Hybrid Material. *Nat. Commun.* **2012**, *3*, No. 1225.
9. Yan, Z.; Ma, L.; Zhu, Y.; Lahiri, I.; Hahm, M. G.; Liu, Z.; Yang, S.; Xiang, C.; Lu, W.; Peng, Z.; *et al.* Three-Dimensional Metal-Graphene-Nanotube Multifunctional Hybrid Materials. *ACS Nano* **2013**, *7*, 58–64.
10. Sun, Z.; Yan, Z.; Jun, Y.; Beitler, E.; Zhu, Y.; Tour, J. M. Growth of Graphene from Solid Carbon Sources. *Nature* **2010**, *468*, 549–552.
11. Ruan, G.; Sun, Z.; Peng, Z.; Tour, J. M. Growth of Graphene from Food, Insects, and Waste. *ACS Nano* **2011**, *5*, 7601–7607.
12. Nikolaev, P.; Bronikowski, M. J.; Bradley, R. K.; Rohmund, F.; Colbert, D. T.; Smith, K. A.; Smalley, R. E. Gas-Phase Catalytic Growth of Single-Walled Carbon Nanotubes from Carbon Monoxide. *Chem. Phys. Lett.* **1999**, *313*, 91–97.
13. Liang, F.; Sadana, A. K.; Peera, A.; Chattopadhyay, J.; Gu, Z.; Hauge, R. H.; Billups, W. E. A Convenient Route to Functionalized Carbon Nanotubes. *Nano Lett.* **2004**, *4*, 1257–1260.
14. Yan, Z.; Lin, J.; Peng, Z.; Sun, Z.; Zhu, Y.; Li, L.; Xiang, C.; Samuel, E. L.; Kittrell, C.; Tour, J. M. Toward the Synthesis of Wafer-Scale Single-Crystal Graphene on Copper Foils. *ACS Nano* **2012**, *6*, 9110–9117.
15. Dresselhaus, M. S.; Jorio, A.; Hofmann, M.; Dresselhaus, G.; Saito, R. Perspectives on Carbon Nanotubes and Graphene Raman Spectroscopy. *Nano Lett.* **2010**, *10*, 751–758.
16. Evans, S.; Thomas, J. M. The Chemical Nature of Ion-Bombarded Carbon: A Photoelectron Spectroscopic Study of Cleaned Surfaces of Diamond and Graphite. *Proc. R. Soc. London, Ser. A* **1977**, *353*, 103–120.
17. Strano, M. S.; Dyke, C. A.; Usrey, M. L.; Barone, P. W.; Allen, M. J.; Shan, H.; Kittrell, C.; Hauge, R. H.; Tour, J. M.; Smalley, R. E. Electronic Structure Control of Single Walled Carbon Nanotube Functionalization. *Science* **2003**, *301*, 1519–1522.
18. Wang, Q. H.; Jin, Z.; Kim, K. K.; Hilmer, A. J.; Paulus, G. L. C.; Shih, C. J.; Ham, M. H.; Sanchez-Yamagishi, J. D.; Watanabe, K.; Taniguchi, T.; *et al.* Understanding and Controlling the Substrate Effect on Graphene Electron-Transfer Chemistry *via* Reactivity Imprint Lithography. *Nat. Chem.* **2012**, *4*, 724–732.
19. Kim, K. S.; Zhao, Y.; Jang, H.; Lee, S. Y.; Kim, J. M.; Kim, K. S.; Ahn, J. H.; Kim, P.; Choi, J. Y.; Hong, B. H. Large-Scale Pattern

Growth of Graphene Film for Stretchable Transparent Electrodes. *Nature* **2009**, *457*, 706–710.
20. Li, X. S.; Cai, W.; An, J.; Kim, S.; Nah, J.; Yang, D.; Piner, R.; Velamakanni, A.; Jung, I.; Tutuc, E.; *et al.* Large-Area Synthesis of High-Quality and Uniform Graphene Films on Copper Foils. *Science* **2009**, *324*, 1312–1314.
21. Reina, A.; Jia, X.; Ho, J.; Nezich, D.; Son, H.; Bulovic, V.; Dresselhaus, M. S.; Kong, J. Large Area, Few-Layer Graphene Films on Arbitrary Substrates by Chemical Vapor Deposition. *Nano Lett.* **2009**, *9*, 30–35.
22. Lin, Y. C.; Lu, C. C.; Yeh, C. H.; Jin, C.; Suenaga, K.; Chiu, P. W. Graphene Annealing: How Clean Can It Be? *Nano Lett.* **2012**, *12*, 414–419.
23. Ci, L.; Song, L.; Jin, C.; Jariwala, D.; Wu, D.; Li, Y.; Srivastava, A.; Wang, Z. F.; Storr, K.; Balicas, L.; Liu, F.; Ajayan, P. M. Atomic Layers of Hybridized Boron Nitride and Graphene Domains. *Nat. Mater.* **2010**, *9*, 430–435.
24. Van der Zande, A. M.; Huang, P. Y.; Cheet, D. A.; Berkelbach, T. C.; You, Y.; Lee, G.; Heinz, T. F.; Reichaman, D. R.; Muller, D. A.; Hone, J. C. Grains and Grain Boundaries in Highly Crystalline Monolayer Molybdenum Disulfide. *Nat. Mater.* **2013**, *12*, 554–561.
25. Dresselhaus, M. S.; Dresselhaus, G.; Eklund, P. C. *Science of Fullerenes and Carbon Nanotubes*; Academic: San Diego, CA, 1996.
26. Artyukhov, V. I.; Liu, Y.; Yakobson, B. I. Equilibrium at the Edge and Atomistic Mechanisms of Graphene Growth. *Proc. Natl. Acad. Sci. U.S.A.* **2012**, *109*, 15136–15140.
27. Wu, Y.; Chou, H.; Ji, H.; Wu, Q.; Chen, S.; Jiang, W.; Hao, Y.; Kang, J.; Ren, Y.; Piner, R. D.; *et al.* Growth Mechanism and Controlled Synthesis of AB-Stacked Bilayer Graphene on Cu-Ni Alloy Foils. *ACS Nano* **2012**, *6*, 7731–7738.
28. Adam, S.; Hwang, E. H.; Galitski, V. M.; Das Sarma, S. A Self-Consistent Theory for Graphene Transport. *Proc. Natl. Acad. Sci. U.S.A.* **2007**, *104*, 18392–18397.
29. Zhou, H.; Yu, W. J.; Liu, L.; Cheng, R.; Chen, Y.; Huang, X.; Liu, Y.; Wang, Y.; Huang, Y.; Duan, X. Chemical Vapour Deposition Growth of Large Single Crystals of Monolayer and Bilayer Graphene. *Nat. Commun.* **2013**, *4*, No. 2096.
30. Li, X.; Zhu, Y.; Cai, W.; Borysiak, M.; Han, B.; Chen, D.; Piner, R. D.; Colombo, L.; Ruoff, R. S. Transfer of Large-Area Graphene Films for High-Performance Transparent Conductive Electrodes. *Nano Lett.* **2009**, *9*, 4359–4363.
31. Saha, A.; Ghosh, S.; Weisman, R. B.; Marti, A. A. Films of Bare Single-Walled Carbon Nanotubes from Superacids with Tailored Electronic and Photoluminescence Properties. *ACS Nano* **2012**, *6*, 5727–5734.
32. Hecht, D. S.; Hu, L.; Irvin, G. Emerging Transparent Electrodes On the basis of Thin Films of Carbon Nanotubes, Graphene, and Metallic Nanostructures. *Adv. Mater.* **2011**, *23*, 1482–1513.
33. Yan, Z.; Peng, Z.; Tour, J. M. Chemical Vapor Deposition of Graphene Single Crystals. *Acc. Chem. Res.* **2014**, 10.1021/ar4003043.
34. Lin, X.; Liu, P.; Wei, Y.; Li, Q.; Wang, J.; Wu, Y.; Feng, C.; Zhang, L.; Fan, S.; Jiang, K. Development of an Ultra-Thin Film Composed of a Graphene Membrane and Carbon Nanotube Vein Support. *Nat. Commun.* **2013**, *4*, 2920.